Experimental analysis of the tensile behaviour of textile reinforced cementitious matrix composites using distributed fibre optic sensing (DFOS) technology

Mohamed Saidi, Aron Gabor

Experimental analysis of the tensile behaviour of textile reinforced cementitious matrix composites using distributed fibre optic sensing (DFOS) technology

Mohamed SAIDI*, Aron GABOR

University of Lyon, University Lyon1, Laboratory of Composite Materials for Construction (LMC2), 82 bd Niels Bohr 69622 Villeurbanne, France.

Abstract

This work presents an experimental study of the mechanical behaviour of textile reinforced cementitious matrix composites (TRCMC) subjected to direct tensile loading. Distributed optical fibres embedded in the core of the composites were used as strain sensors. The measurements were based on the Rayleigh backscattering principle. The sensors were able to measure the strain in the specimen during the test at different locations because of their spatial resolution and reduced dimensions and thus make it possible to analyse and identify the behaviour of the matrix, the textile, and the textile/matrix interface. Six configurations were tested and analysed in this study: two types of matrices with three reinforcement ratios.

The local and global behaviours were analysed, and the test results during the three typical stages of the mechanical behaviour of TRCMC composites are explained. The parameter controlling the behaviour of the crack propagation phase is identified, and an explanation of its influence on crack distribution is highlighted. The validity of the law of mixtures and the hypotheses of the textile/matrix interface were examined and compared to experimental results. The influence of the reinforcement ratio was also identified. The obtained results allow a better understanding of the local and global mechanical behaviours of TRCMC composites and the assessment of present theoretical hypotheses in literature related to these behaviours.

Keywords

Textile Reinforced Concrete; cementitious composite matrix; optical fibre; strain sensor; reinforcement/matrix interface; internal mechanical behaviour.

*Corresponding author: Tel: +33 4 72 69 21 30, Fax: +33 4 78 94 69 06
E-mail addresses: mohamed.saidi@univ-lyon1.fr (M. SAIDI), aron.gabor@univ-lyon1.fr (A. GABOR).

1. Introduction

In the field of civil engineering, the reinforcement, repair, and rehabilitation of existing buildings and structures have become a major requirements in recent years. One widely followed solution is the use of composite materials as a reinforcement method, in particular, textile reinforced cementitious matrix composites (TRCMCs) [1–6]. These composites are obtained by the insertion of a high tensile-performance textile within a cementitious matrix. This combination provides composites with mechanical performance adaptable to the requirements of reinforcement or rehabilitation [7,8].

The mechanical tensile behaviour of TRCMCs has been the subject of several studies [1,8–11] that have concluded it is generally composed of three phases:

- Phase 1: called the pre-cracking zone, is characterised by a linear behaviour in terms of stress and strain with a stiffness E_1 close to that of the matrix. This zone can be limited by a strain ε_1 and a maximum stress σ_1 equal to the ultimate stress of the matrix in tension (Fig. 1).
- Phase 2: called the crack propagation zone, begins after the occurrence of the first crack in the TRCMC composite and is characterised by a succession of transverse cracks perpendicular to the direction of the applied tensile load. This area can be characterised by a low equivalent stiffness (Fig. 1).
- Phase 3: called the post-cracking zone, is characterised by a stiffness greater than that of the second zone and smaller than that of the first zone. This zone is governed by the mechanical properties of the reinforcement and includes the equivalent stiffness E_3 and the ultimate stress σ_3 (Fig. 1). In this zone, the opening of cracks occurred during the second phase increase with the increase of the applied load on the composite.

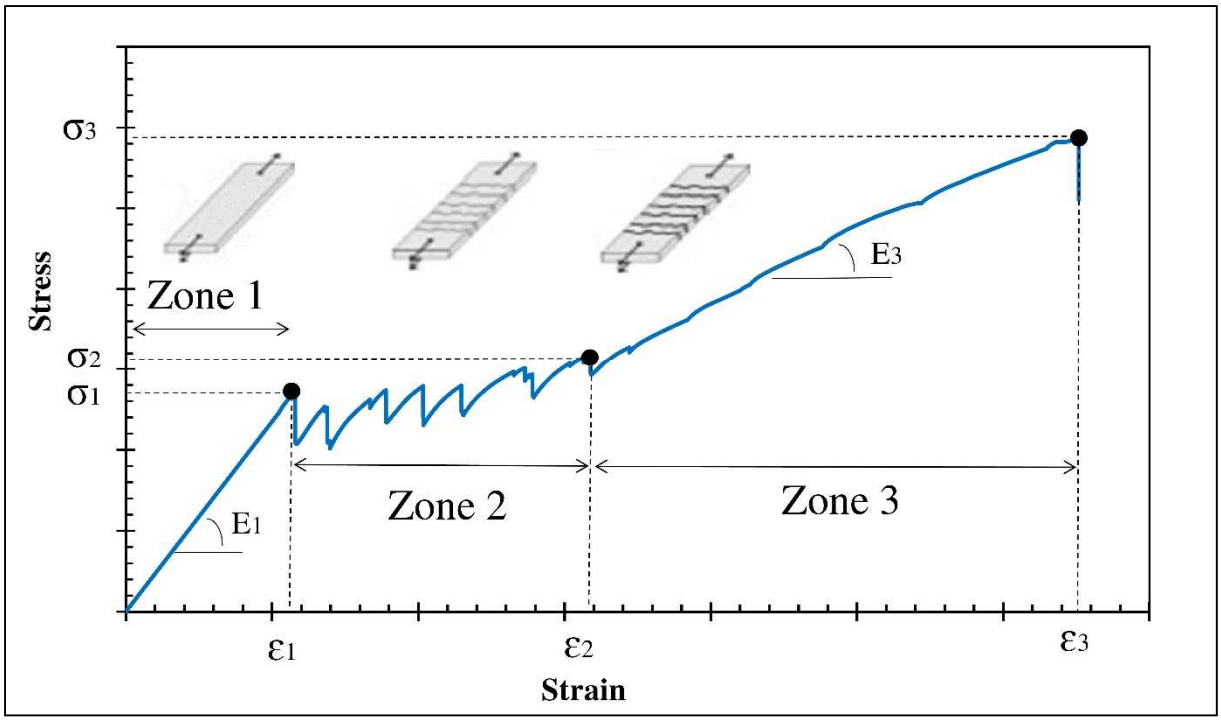

Fig. 1: Tensile behaviour of a typical TRCMC

The global mechanical behaviour of TRCMCs is studied by different measurement techniques with or without contact by measuring the strain and stress field on the surface of specimens. The most used techniques are: extensometry by strain gauges or displacement sensors such as linear variable differential transformer, digital image correlation, and laser extensometer [12–16]. From experimental results, the internal behaviour of these composites is modelled using continuum and fracture mechanics approaches. These models are developed with assumptions estimating the micro-mechanical parameters governing the textile/matrix interaction of TRCMCs [17–19]. The parameters generally include the shear stress at the textile/matrix interface and the load transfer length. Some authors assume that the shear stress at the interface is constant along the anchor length of the reinforcement [17], others consider that it decreases linearly from the most stressed part of the reinforcement, and some assign parabolic or exponentially decreasing shapes to the distribution of the supposed stress at the interface. Experimentally, to date, no study has investigated the direct local measurement of interface stress. Research has shown that, in addition to the reinforcement and matrix, textile preimpregnation influences the behaviour at the interface, stating that the global behaviour of TRCMCs is improved by preimpregnating the reinforcement [20–22]. Similarly, for other parameters influencing the behaviour of TRCMCs, their quantification is limited to classical experimental measurements of the displacement or strain field on the surface of a specimen.

Optical fibre measurement technology is used in several fields, including civil engineering. Optical fibre is used as a tool for health and safety monitoring of structures because of its geometric (small size, sensor length, flexibility, and light weight) and metrological advantages (accuracy, high recording frequency, millimetric spatial resolution, and sensitivity). These sensors have been the subject of numerous studies, including their behaviour at the core of reinforced concrete beams [23–27], their ability to detect internal cracks in concrete structures [28] and the stress transfer mechanisms between the components of optical fibre sensors [29].

The use of optical fibre measurement in composite materials has been the subject of several experimental investigations [30–32], in particular, Bragg's grating technique. Thermoplastic matrix composites have been studied using optical fibres [33] and textile-reinforced polymer matrices such as fibre-reinforced plastic [34–36], but no experimental studies with optical fibre sensors have been dedicated to cementitious matrix composites. The intrusiveness of optical fibre and its influence on the behaviour of composites was evaluated [37] and indicated that for a quasi-static test, optical fibre sensors have no impact on either the behaviour of composites or damage propagation. The integrity of the optical fibres during testing and their bond with the cementitious mortar was tested and evaluated [32,38]. The bonding was verified both for elastic and post-cracked domain. For the study [32], the theoretical and experimental results of an optical fibre embedded in a cementitious matrix beam, tested in three-point bending were compared. Then the cracking was analysed by a tensile test, placing an optical fibre and strain gauges on the surface of a cementitious matrix composite and comparing the results of the two measurement techniques before, during and after crack propagation. For the study [38], an optical fibre is glued to the surface of a concrete beam in four locations with four different adhesives. The beam is tested in three-point bending, then the optical fibre results are compared before and after cracking with those of the strain gauges on the surface of the beam, to study the effect of the type of adhesive.

To the best of the authors' knowledge, no experimental studies have investigated the internal local behaviour of TRCMCs in tension. The objective of this work is to experimentally study the internal behaviour of TRCMCs and to visualize, explain, and clarify the tensile behaviour and its scientific problems based on local measurements in the core of a material. In addition, we present an experimental reference to evaluate the validity of some existing models. For this purpose, distributed strain sensors of optical fibre [39] were embedded in a TRCMC. The measurements based on the Rayleigh backscattering principle allowed us to obtain the local

behaviour of the matrix, the textile reinforcement, and the deduction of their interaction at the interface.

2. Experimental program

This work was based on an experimental study of the direct tensile test of TRCMCs with embedded optical fibres. The tests were conducted through an experimental protocol presented in the following sections.

2.1.Tensile testing machine

The tensile test applied to composite specimens was performed using a Zwick universal testing machine shown in Fig. 2 with a maximum load capacity of 65 kN, an accuracy of the load cell of 0.2% with a resolution of 0.01 N and an accuracy of the displacement cell of 0.06% with a resolution of 0.001 mm. The entire tensile test was controlled by a data acquisition system that configured the test and recorded the applied load. The test was controlled in displacement with a velocity of 100 µm/min. To reduce the effect of parasitic bending owing to possible geometric imperfections of the specimen, two ball-joint loading heads were used to maintain and transmit the load from the Zwick machine to the TRCMC specimen (Fig. 3) [7].

2.2.Optical data acquisition

An optical distributed sensor interrogator device (ODiSI-B, Luna) was used to acquire the strain measured by the optical fibre. This instrument was based on the optical frequency domain reflectometry–Rayleigh principle [39] and had a random error of less than 0.1 GHz or approximately 1 με. It managed and programmed all the parameters related to the optical fibre (acquisition ratio, spatial resolution, and calibration) and instantly visualised and recorded the strain distribution along the optical fibre during testing. For our study, we chose a 2-Hz acquisition ratio and a spatial resolution of 2.6 mm over the entire range of the optical fibre (2 m).

The characteristics of the ODiSI-B interrogator and optical fibre used in this study are summarised in Table 1 and Table 2**Error! Reference source not found.**. C_ε^R and C_T^R are calibration coefficients allowing to link the Rayleigh spectral shift to the strain and temperature of the measured material.

Table 1: Properties of the ODiSI-B interrogator

C_{ε}^{R} (Hz/με)	C_{T}^{R} (Hz/°C)	Maximum data acquisition ratio (Hz)
-6.679	0.638	100

Table 2: Properties of optical fibre

Type of the optical fibre	Glass core diameter (με)	Glass cladding diameter (με)	Type of the protective coating	Diameter the protective coating (με)	Sensing length (m)	Maximum and minimum operating temperature-sensing region (°C)	Spatial resolution (mm)
Polyimide coated low bend loss fibre	9	125	Polyimide coatings	250	2	220, -40	2.6

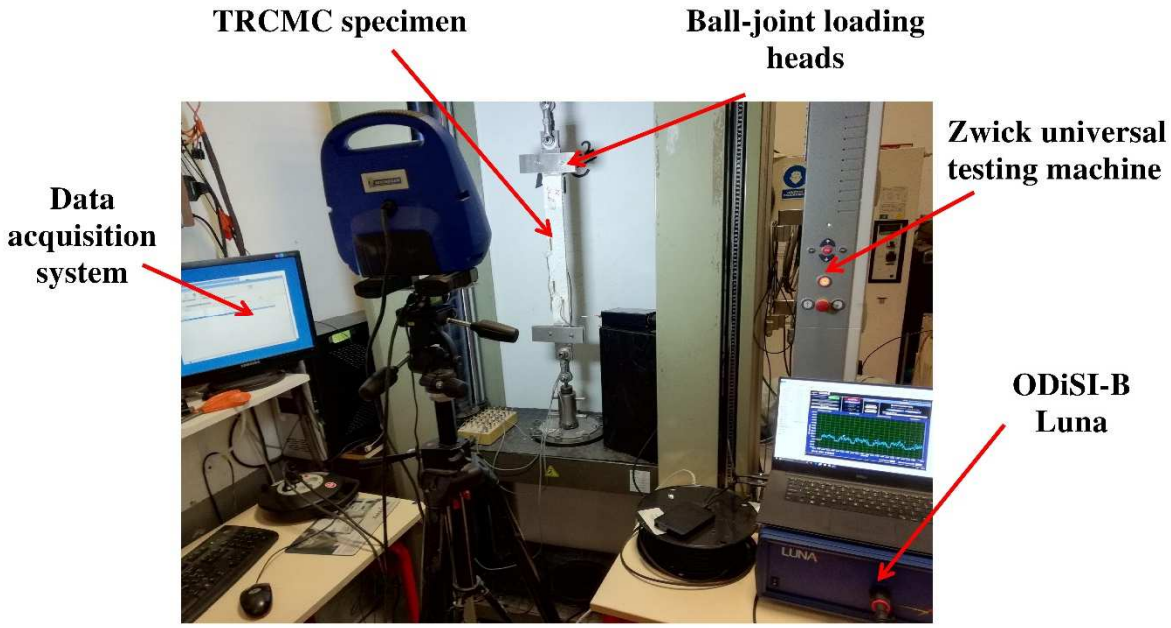

Fig. 2: Experimental setup for tensile testing and measurement by optical fibre.

Fig. 3: Ball-joint loading heads used to transmit the load from the Zwick press to the TRCMC specimen.

3. Specimens

3.1.Materials

The TRCMC studied in this work was a combination of two components: a self-sealing liquid-cement matrix and a reinforcement glass textile. Six configurations were studied: two types of matrices with three reinforcement ratios V_f (2.4%, 4.8% and 7.2%). The mechanical properties of the two components are described in the following subsections.

3.1.1. Self-placing liquid-cement matrix

To avoid any possible damage to the optical fibre, its positioning and embedding inside the composite required particular attention to the choice of materials used and the preparation methodology. In addition, it was necessary to ensure a good coating on the optical fibre by the matrix to provide satisfactory transmission of the measured information. To this end, two self-placing, liquid, ettringitic cementitious matrices were used to provide good workability and shape retention. They were characterised in the laboratory using standard tests [40]. The mechanical properties of the cementitious matrices M1 and M2 are shown in Table 3.

Table 3: Mechanical properties of cementitious matrices M1 and M2 tested in the laboratory

		σ_{ultime} Compression (MPa)	σ_{ultime} Tension (MPa)	ε_{ultime} Compression (µm/m)	ε_{ultime} Tension (µm/m)	E_c Compression (MPa)	E_t Tension (MPa)
Matrix M1	Average	31.2	3.5	2,350	300	13,000	10,700
	Standard deviation	1.10	0.20	160	27	454	316
Matrix M2	Average	40	4.5	3,000	400	13,000	14,000
	Standard deviation	1.57	0.36	230	34	507	492

3.1.2. Reinforcement textile

The textile reinforcement used in the TRCMC made of alkali-resistant glass, coated with a polymer modified, had a grid shape with a mid-yarn grid spacing of 5 × 5 mm. The yarns in the warp and weft direction had weights of 272 Tex and 2,400 Tex, respectively. Table 4 summarizes the main geometrical and mechanical properties of the textile measured in the laboratory. The cross-section of the yarn in the weft direction, which is the direction subjected to the tensile load, was considered of an elliptical shape, with a major radius denoted as 'R' and a minor denoted as 'r', respectively (Table 4). The mechanical characterisation of the textile yarns is done following a test protocol developed in our laboratory. It consists in testing in pure tension a 35 cm long yarn as shown in Fig. 4, with two aluminium plates at both ends (as in the case of TRCMCs). The stress is obtained by dividing the applied force by the cross-sectional area of the yarn. The displacement is obtained by using a laser sensor that measures the relative displacement between two zones on the yarn, which are initially spaced 10 cm apart. The strain is therefore deduced by dividing the measured displacement by the initial distance between these two measurement spots.

Table 4 : Geometrical and mechanical properties of the yarns in the weft direction of the AR glass textile

	Radius of yarn (R/r) (mm)	Tensile strength of yarn (MPa)	Young's modulus of AR glass fibre (MPa)	Maximum strain (%)	Textile weight (g/m²)
Average	1.67/0.40	520	35,000	1.5	525
Standard deviation	0.11/0.02	48	3,180	0.12	-

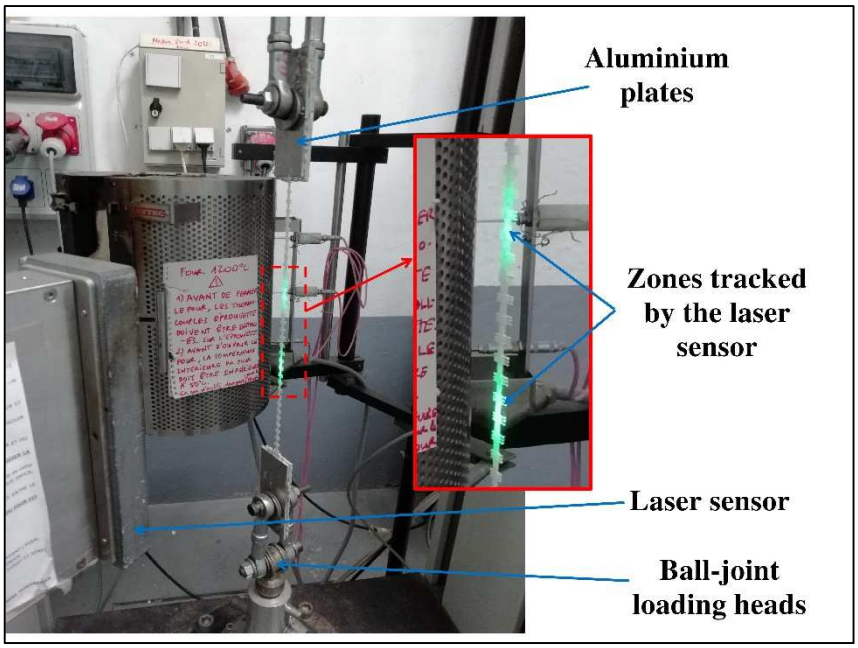

Fig. 4: Experimental protocol for the mechanical characterisation of the yarns of a reinforcing textile.

3.2.Specimen preparation

To measure the internal strain of the TRCMC, the optical fibre was placed in six different positions in the core of the composite. For this purpose, an effective measuring length of 20 cm was set for the six positions with five external loops of 10 cm each.

The form of the TRCMC specimens was chosen based on studies reported in literature [7,12,32,41]. The form of the specimens was parallelepipedic with approximate dimensions of 600 × 50 × 10 mm (length × width × thickness) with an average of the total cross-sectional area of the composite $S_c = 550 \pm 15$ mm², as shown in Fig. 6 and Fig. 7.

The preparation is detailed on [32], and consisted principally in the embedding of the optical fibre at six different positions in the composite as follows:

- TRCMC with a single reinforcement layer: two segments of optical fibre between the textile reinforcement and the upper surface of the specimen, two segments on the textile reinforcement, and two between the textile reinforcement and the lower surface of the specimen.
- TRCMC with two reinforcement layers: two segments of optical fibre on the lower textile reinforcement, two segments in the matrix between the two textile reinforcement layers, and two segments on the upper textile reinforcement of the specimen.

- TRCMC with three reinforcement layers: two segments of optical fibre on the lower textile reinforcement, two on the textile reinforcement in the middle, and two on the upper textile reinforcement of the specimen.

A mould was prepared by superposing four layers of 2 mm thick polyvinyl chloride plastic. This superposition allowed us to place and centre both the textile reinforcement and the optical fibre in different positions. Between each two superposed plastic plates, depending on the number of reinforcement layers, either a layer of textile reinforcement was positioned or a 0.7 mm sewing thread was stretched (for more details, see [32]). For the strain measurement of the textile reinforcement, a segment of the optical fibre is bonded on the top of a yarn of the textile layer using a cyanoacrylate glue along the textile in the direction of the applied load. For matrix strain measurements, at the position where there is no textile reinforcement, the segments of the optical fibre were locally attached using sewing twine knots every 5 cm to the stretched sewing thread previously placed at the desired location. Where a reinforcement layer is placed, and in addition to the segment of the optical fibre bonded to the textile, another segment was positioned on the reinforcement textile, then locally attached to the textile using sewing twine knots every 5 cm. This means that for each reinforcement layer, two segments of optical fibre are placed on it (Fig. 5), one glued to have the textile strain, and another simply placed to have the matrix strain in the vicinity of the textile.

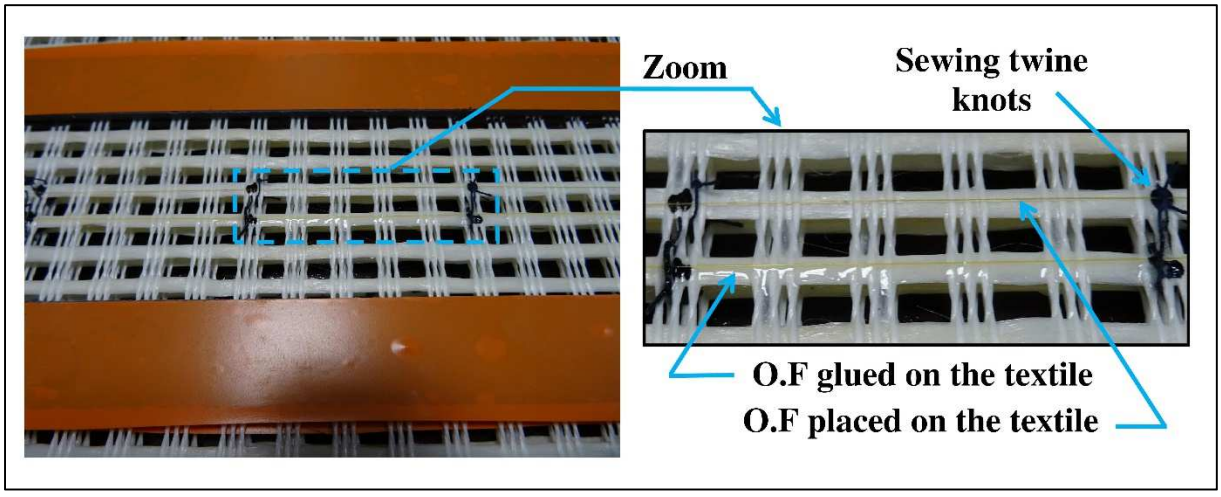

Fig. 5: Positioning of the optical fibre on the textile reinforcement

To form a loop, the optical fibre was removed from the mould and protected with a plastic sleeve. The external protection prevented accidental damage to the optical fibre and allowed the detection of the unloaded segments. This facilitated the post-processing with the identification of the correct abscissa of every segment of the optical fibre.

Once the mould was prepared and the positioning of the optical fibre was complete, the matrices were prepared and poured into the moulds. The moulds were slightly vibrated manually during and after pouring to ensure a good embedding of the optical fibre and textile reinforcement and to evacuate all air bubbles from the matrices.

Once cast, the TRCMC specimen was covered with a plastic film for two days to facilitate the cement hydration and then cured at room temperature, then demoulded. Just after demoulding, two aluminium plates were bonded with epoxy resin at each of the two ends of the specimen. These specimens were then stored at room temperature until the test day. Cementitious matrix suppliers specify that the curing time is 7 days for matrix M1 and 15 days for matrix M2. The tests of matrices M1 and M2 (Table 3) and tensile tests of TRCMCs were made directly after these curing times.

When the TRCMC specimen is placed in the testing machine, two other aluminium plates compressively clamp the plates glued to both ends of the specimens as shown in Fig. 2. This is done to increase the bond between the textile reinforcement and the matrix at the ends covered by the aluminium plates, in order to avoid slippage and delay it, to get as close as possible to the failure stress of the specimen.

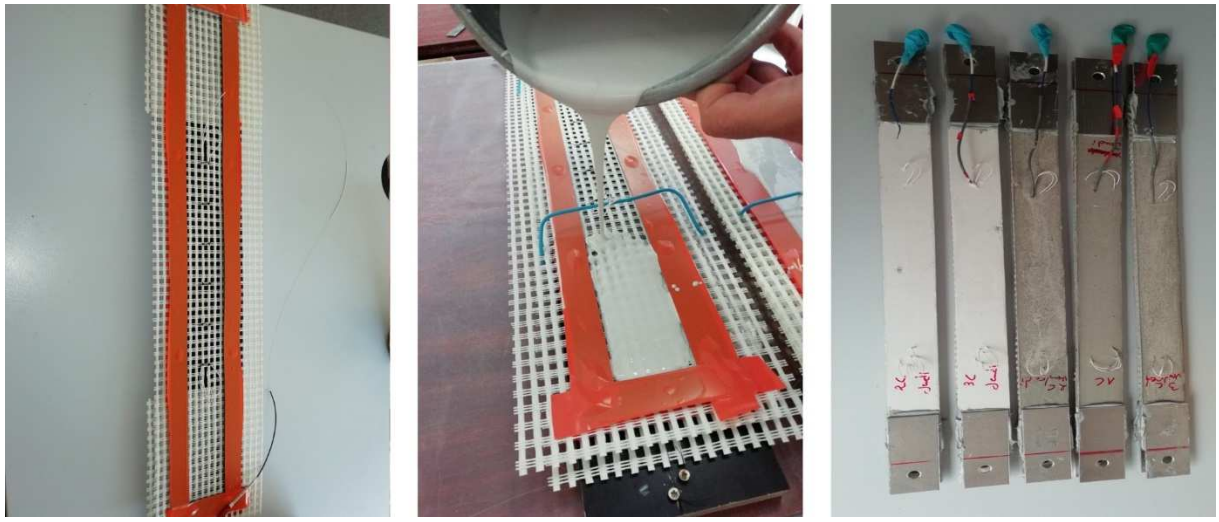

a b c

Fig. 6: Preparation of TRCMC specimens: (a) preparation of mould with optical fibre, (b) pouring of matrix, and (c) demoulding and bonding of aluminium plates.

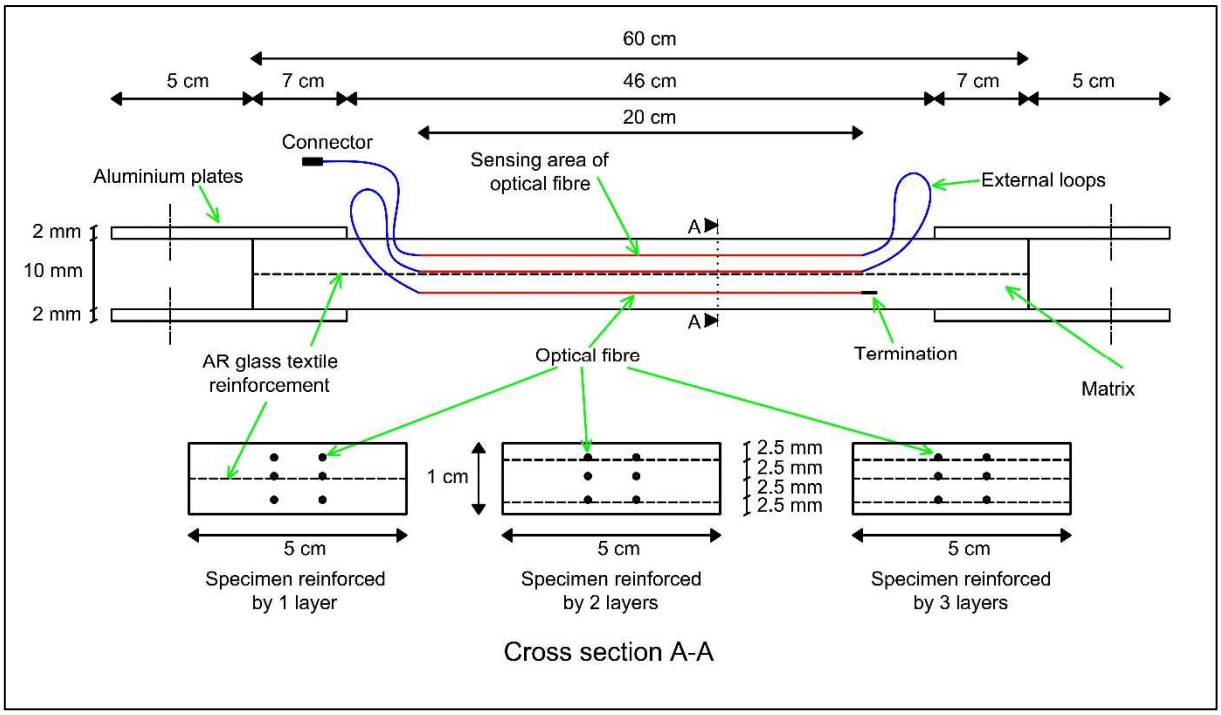

Fig. 7: Diagram of geometric characteristics of TRCMC specimens with optical fibre positions.

3.3.Repeatability of the results

To ensure the repeatability of results, four tests per configuration were performed: three specimens were equipped with a linear variable differential transformer (LVDT) attached to the aluminium plates, and one specimen per configuration is equipped with optical fibre. The aim is to compare the global behaviour to ensure its repeatability, then only one specimen per configuration is instrumented by optical fibre for the analysis of the local behaviour of the TRCMC. This choice is made for cost effectiveness reasons of the optical fibre equipment. Furthermore, taking into account the fragility of the optical fibre and the presence of external optical fibre loops on the surface of the specimens, those specimens were not instrumented with external LVDT. The overall displacement field was measured by the displacement of the crossbeam of the testing machine. The testing machine is highly precise (accuracy of the displacement cell is 0.06% with a resolution of 0.001 mm). Nevertheless, it should be noted that for most of the tested specimens, the ultimate stress and strain (σ_3 and ε_3) does not correspond to the failure of the specimen, but rather to the sliding of the textile reinforcement at the location of the aluminium plates. For this reason, the ultimate stress and strain in Table 5 are not representative, non-repeatable and their standard deviations are high. For this work, this stress and strain will not be considered.

Table 5: The stress and the corresponding strain at the end of each zone of the global tensile behaviour ("M" denotes matrix and "L" denotes layer; for example: "M1-2L" denotes matrix M1 reinforced by 2 layers)

Specimen	Value	σ_1 (MPa)	σ_2 (MPa)	σ_3 (MPa)	ε_1 (µm/m)	ε_2 (µm/m)	ε_3 (µm/m)
M1-1L	Average	3.58	4.86	6.13	278.67	1,509	3,701
	Standard deviation	0.07	0.39	1.82	12.06	55.65	1,300
M1-2L	Average	3.71	4.78	8.28	356.33	1,096	3,232
	Standard deviation	0.17	0.25	1.05	31.01	98.81	630.71
M1-3L	Average	3.66	6.09	12.67	300.33	1,098	3,853
	Standard deviation	0.23	0.49	1.00	7.23	104.15	440.19
M2-1L	Average	4.44	5.52	6.93	356.00	1,525	3,188
	Standard deviation	0.22	0.84	2.96	13.23	143.17	2,756
M2-2L	Average	4.83	6.27	12.26	428.50	1,183	4,810.75
	Standard deviation	0.58	0.79	2.08	58.54	219.91	1,128
M2-3L	Average	4.49	7.26	18.15	400.50	1,032	5,244
	Standard deviation	0.05	0.40	0.78	27.58	31.82	166.88

4. Experimental results

4.1.Distribution of normal strain in TRCMC during test

This section presents the experimental results of the distribution and evolution of normal strain at the core of the TRCMC during the tensile test. The choice of a spatial resolution of 2.6 mm for a 2-m long optical fibre provided 770 measuring points of strain along the fibre. Thus, for an effective measurement area of 20 cm per longitudinal position, 77 measuring points of strain were obtained for each segment.

Fig. 8 provides an overview of the behaviour of the matrix and textile reinforcement within the TRCMC: Fig. 8-a before cracks appear, and Figs. 5-b, c, and d during crack propagation. The matrix strain shown in Fig. 8 is derived from the segment of the optical fibre embedded in the matrix in the middle of the M2-2L specimen. The textile strain is obtained from the segment of the optical fibre bonded to the textile of the upper part of the M2-2L specimen. Before cracking, the strain of the textile and the matrix were approximately identical, while after the appearance of cracks, peaks of strain were recorded at the crack locations, and a gradual increase of strain was observed for the textile and a decrease for the matrix over a length denoted as δ_o. The phenomenon of the 'positive' spike of the matrix strain in the location of the crack which in contrast with the strain trend described in the text will be explained in the following section (i.e. sub-section 5.2). The results in Fig. 8 correspond to the composite using the M2 matrix reinforced with two layers of textile. Similar mechanisms and behaviours were found for the other tested configurations.

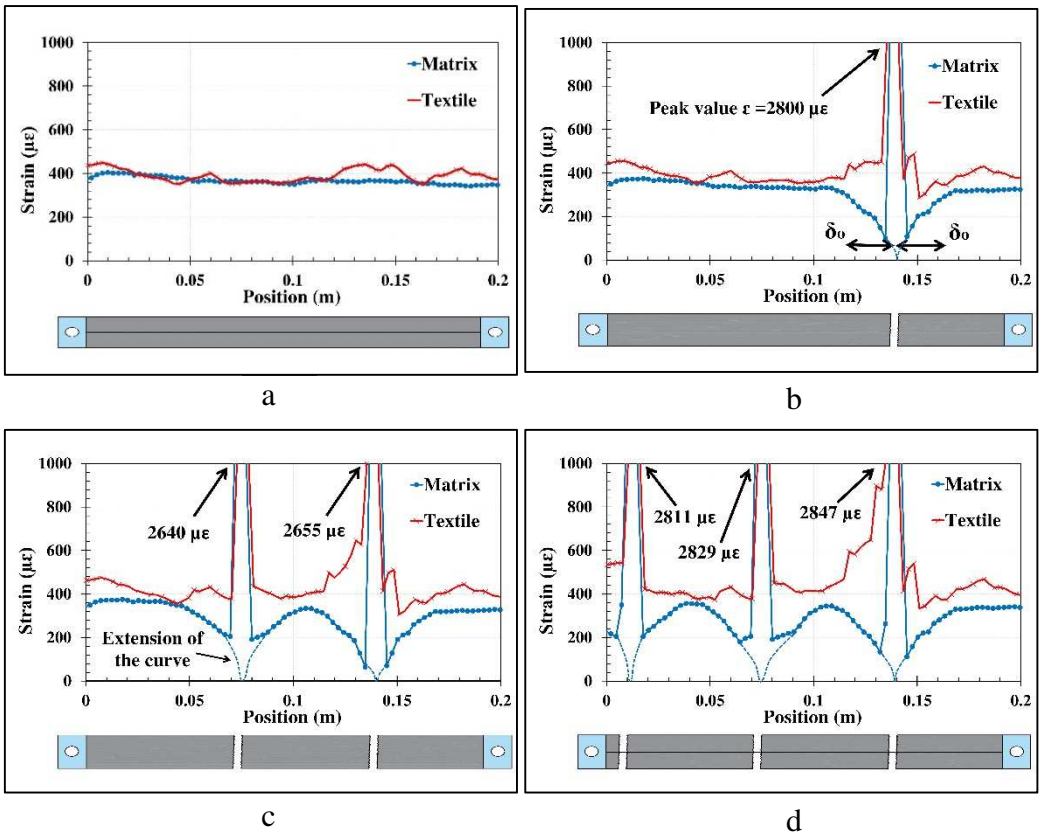

Fig. 8: Experimental results of the distribution of strain in the matrix and textile of the TRCMC specimen M2-2L with the applied load F: (a) before cracking (F = 2680 N), and during occurrence of (b) first crack (F = 2495 N), (c) second crack (F = 2500 N), and (d) third crack (F = 2585 N).

4.2.Distribution of shear stress at textile/matrix interface of TRCMC specimen during test

The calculation method of the distribution of shear stress at the textile/matrix interface τ(x) and its evolution during the test are described in Fig. 9 and Fig. 10, respectively.

This parameter was deduced using the strain gradient in the matrix. Once the matrix cracked, the stress applied to the specimen was fully supported by the textile at the crack location and then redistributed from the textile to the matrix gradually over the distance δ_o on both sides of the crack position (Fig. 9). Therefore, the stress in the matrix after cracking was the result of the load transfer from the textile to the matrix. The matrix stress was deduced from the matrix strain measured by the optical fibre. In the case of TRCMC reinforced with one or two layers of textile reinforcement, the matrix strain is obtained by the segments of the optical fibre in the matrix. In the case of the three layers, the matrix strain is obtained by the segment of the optical fibre simply placed on the textile (see sub-section 3.2, Fig. 5). Then, given the geometric characteristics of the tested specimen, the force in the matrix was calculated. By dividing this

force by the lateral outer surface of longitudinal fibres of the textile, assuming that all these fibres work identically, the shear stress at the interface was obtained.

Over a measurement length of dx = x(i+1) – x(i), the force gradient in the matrix is

$$\Delta F_m(x) = F_{m(i+1)} - F_{m(i)} = S_m \times \Delta\sigma_m(x) = S_m \times E_m \times \Delta\varepsilon_m(x). \quad \textbf{Eq. 1}$$

Therefore, the shear stress at the interface is

$$\tau(x) = \frac{\Delta F_m(x)}{P_f \times N_{bf} \times dx} = \frac{S_m \times E_m \times \Delta\varepsilon_m(x)}{P_f \times N_{bf} \times dx}, \quad \textbf{Eq. 2}$$

where dx corresponds to the spatial resolution of the optical fibre equal to 2.6 mm, S_m is the cross-sectional area of the matrix, E_m is the Young's modulus of the matrix in tension, $\Delta\varepsilon_m(x)$ is the strain gradient between two successive measurement points of the optical fibre, P_f is the perimeter of a yarn in the textile reinforcement, and N_{bf} is the total number of yarns in the TRCMC specimen.

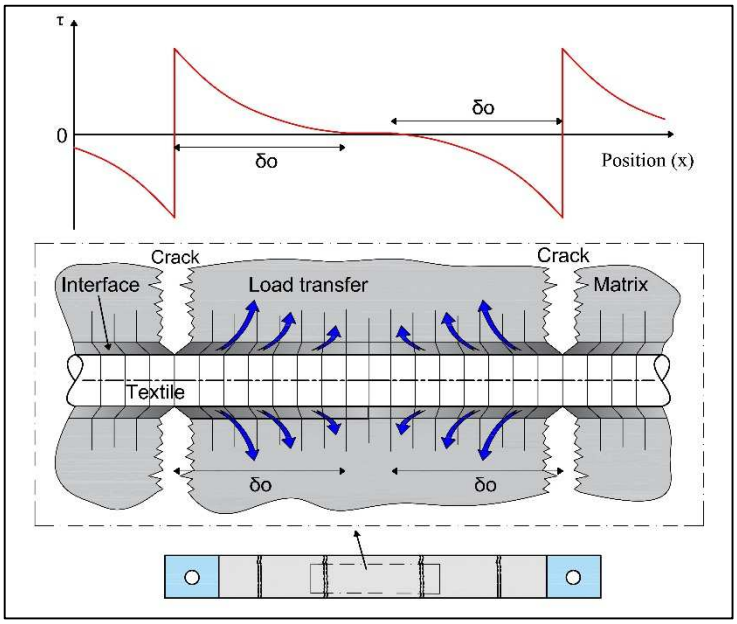

Fig. 9: Diagram of evolution of shear stress at interface and textile/matrix interaction after cracking.

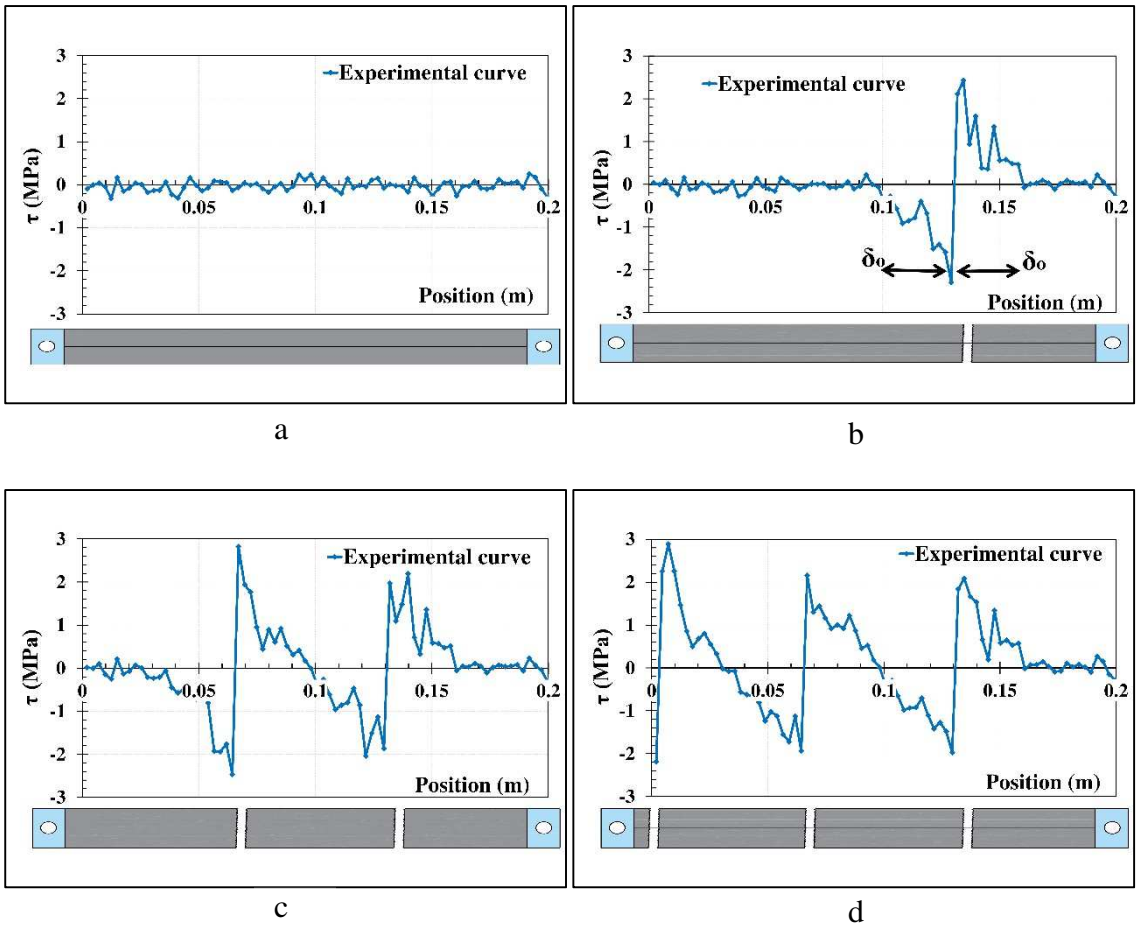

Fig. 10: Experimental results of progress of shear stress at textile/matrix interface along the TRCMC specimen M2-2L: (a) before cracking, (b) at first crack, (c) at second crack, and (d) at third crack.

4.3.Global and local mechanical behaviour of TRCMC components

To obtain an overview of the local mechanical behaviour at different positions of the two components of the TRCMC and its global behaviour, four measurements are presented in terms of the stress and strain curves in Fig. 11. The solid line (grey) illustrates the behaviour of the matrix in an uncracked area, the dotted line (tan) illustrates the behaviour of the textile in an uncracked area, the large-dashed line (blue) illustrates the behaviour of the textile at the crack location, and the global behaviour of the specimen derived directly from the displacement of the Zwick machine is represented by a dashed line (green). These results correspond to the TRCMC made with the M2 matrix reinforced with two layers of textile reinforcement. The observations obtained from these results and the different forms of curves presented in Fig. 11 can be generalised to all other TRCMCs. The stress presented in Fig. 11 corresponds to that in the composite, i.e. the applied total force divided by the total cross-sectional area of the composite.

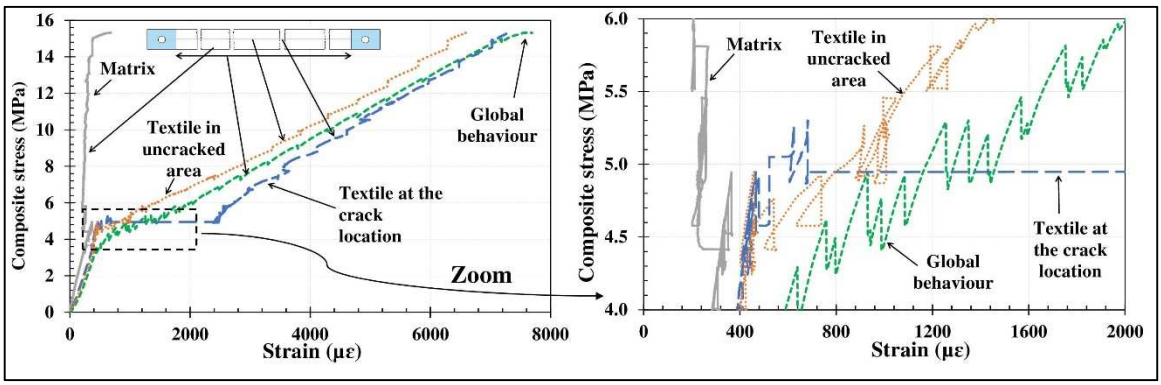

a b

Fig. 11: Comparison of experimental results of mechanical behaviour of matrix, of textile at the cracked and uncracked regions, and of global behaviour of the specimen M2-2L: (a) global view and (b) focus on the second phase of behaviour.

4.4.Mechanical behaviour of textile reinforcement at core of TRCMC

A comparison of the mechanical behaviour of the textile within the TRCMCs depending on the type of matrix is presented in Fig. 12 (Fig. 12-a: matrix M1 and Fig. 12-b: matrix M2) along with the number of reinforcement layers, i.e. the reinforcement ratio. The aim was to analyse the slope of the third phase of the TRCMC mechanical behaviour and assess the behaviour of the textile at the core of the cementitious composite, then to compare it with the tensile behaviour of a single textile. This will verify the accuracy of the theoretical assumptions of several studies that assimilate the behaviour of the third TRCMC zone to that of the textile alone and that assume that the matrix is no longer loaded in tension in this zone. The maximum strains recorded for M1 and M2 in Fig. 12 are different due to the sliding of the textile in the matrix at the positions of the aluminium plates as indicated in sub-section 3.3.

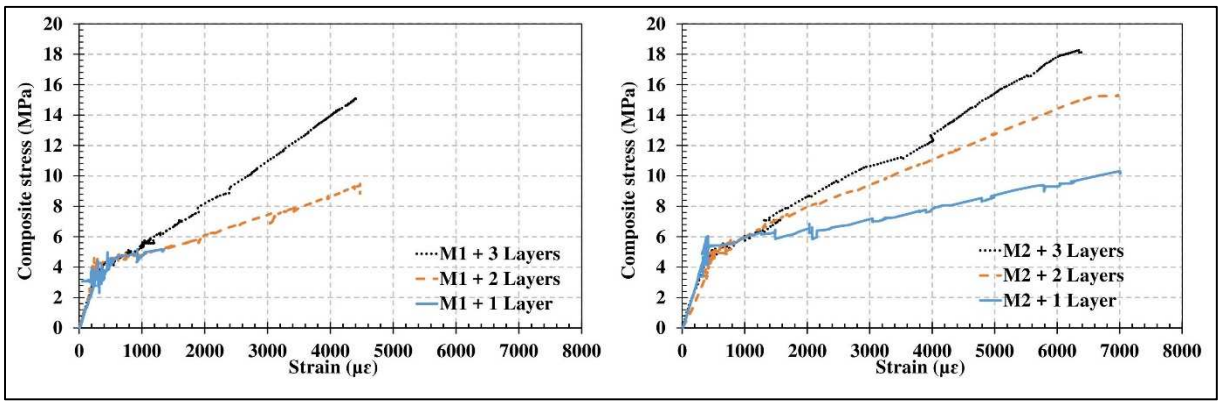

a b

Fig. 12: Experimental results of internal mechanical behaviour of textile at core of TRCMC for the two matrices and the three reinforcement ratios: (a) matrix M1 and (b) matrix M2.

The strain at each load step in Fig. 12 is the average of the values corresponding to each textile strip (layer). Indeed, for each configuration, an average is calculated along each optical fibre segment glued to the textile, and then a total average is calculated between the averages of each textile strip. Fig. 13 shows the average of each textile layer and the total average for TRCMC M1-3L. It can be observed that the behaviour of the three textile layers is almost identical, and it can be concluded that the applied stress to the composite is uniformly distributed over the reinforcement layers. These results can be generalised for all the other configurations tested.

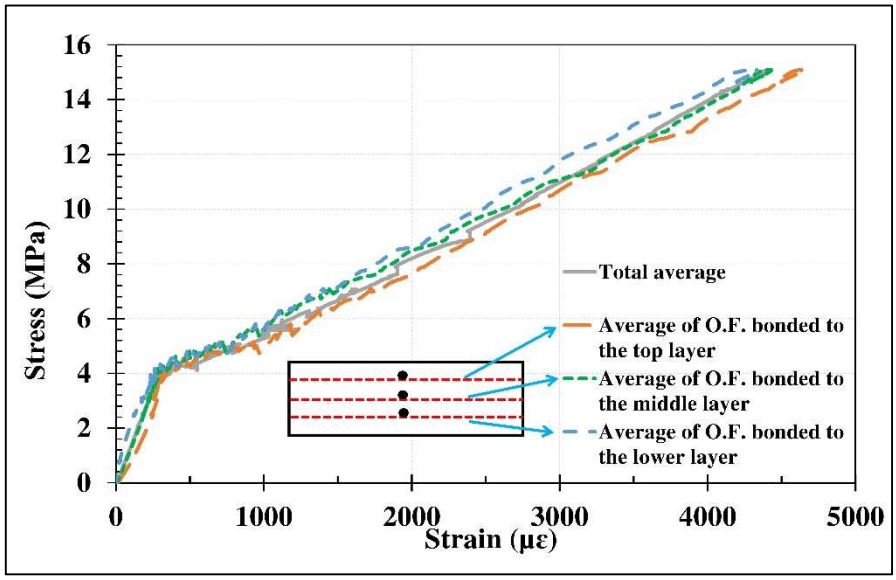

Fig. 13: Strain average of each optical fibre segment along a reinforcement layer for the M1-3L specimen and total average of the three layers

4.5.Cracking diagram and failure mode of TRCMC composite

The cracking mode of TRCMCs in tension is characterised by a random appearance of unevenly spaced transversal cracks perpendicular to the loading direction. At the end of each tensile test, the locations of the cracks of the tested specimens were identified and marked for good visibility (Fig. 14).

For the six tested TRCMC configurations, failure occurred at the interface between the matrix and the textile reinforcement at one of the two ends of the specimen under the aluminium plates. This implies that the bond strength of the textile/matrix interface in this region was lower than that of the textile's tensile strength. Given this observation, the maximum strength of the TRCMC tested in this study driven by the textile/matrix interface was underestimated, and therefore the maximum stress of the TRCMC was not studied in this work.

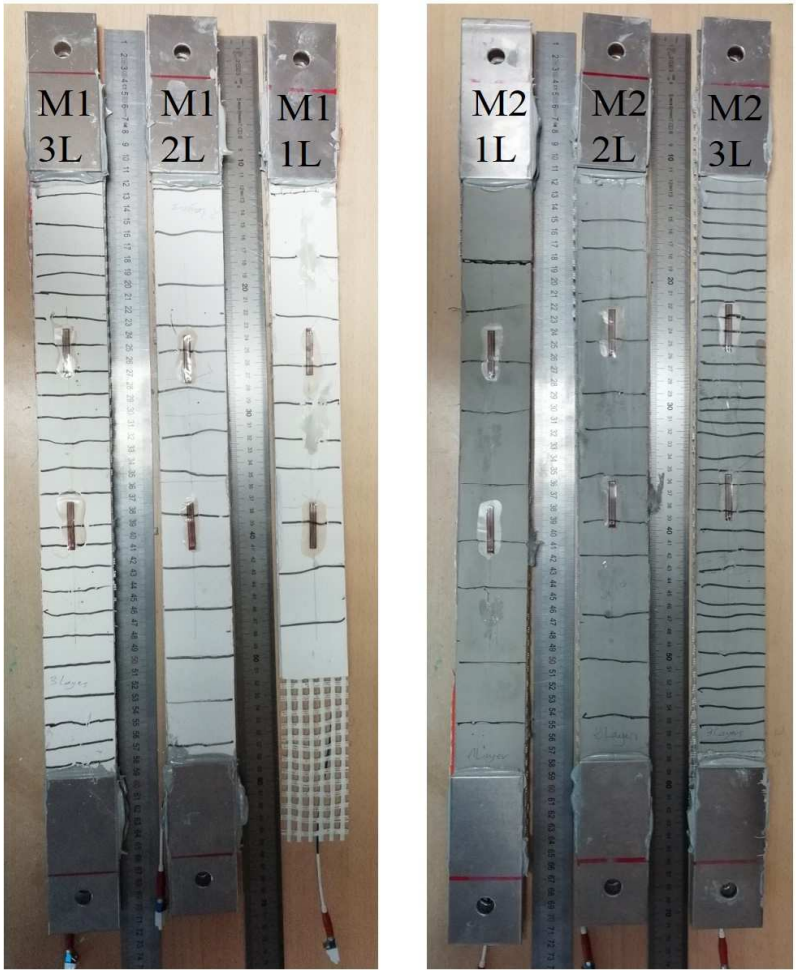

Fig. 14: Cracking diagram of specimens after tensile tests with three reinforcement ratios (L denotes layer): (a) Matrix M1 and (b) Matrix M2.

5. Discussion

To properly discuss the experimental results, each of the three zones of the TRCMCs' mechanical behaviour was analysed separately.

The discussion of the experimental results is based on the assumption that the behaviour of the matrix over its entire cross-section is homogeneous, and the behaviour of the longitudinal yarns of the textile is identical.

5.1.First zone: pre-cracking zone

Generally, from the strain distribution in the matrix and textile during the tensile test of the TRCMC (Fig. 8), it can be deduced that for the pre-cracking zone, the strain profile was constant along the specimen (Fig. 8-a). As we had the same strain in the textile and the matrix over the length of the specimen, one can conclude that any parasitic bending that may have resulted from geometric defects was insignificant. Thus, the strain in the matrix and the textile were approximately the same.

Likewise, according to Fig. 11, the pre-cracking phase exhibited a quasi-linear behaviour in terms of the stress/strain curves. Thus, by comparing the curves of the matrix and textile in the first zone (pre-cracking zone) in Fig. 11, the behaviour of the matrix and the textile in this zone was almost identical, and almost the same strain value was recorded for these two components for a given force.

Based on the results related to the global and local mechanical behaviours of the TRCMC, it can be concluded that for the pre-cracking zone, the law of mixtures was applicable, i.e., the assumption of a perfect matrix/textile interface is valid, and therefore the strain on the reinforcement was equal to that of the matrix in the first zone.

At the interface level, since the two components of the TRCMC were elongated in the same quantity and in the same way, no friction or differential strain was developed at the interface, and therefore the stress at the interface was almost zero as shown in Fig. 10-a. Thus, the distribution of the strain in the matrix in the longitudinal direction of the specimen was quasi-linear (Fig. 8-a), yielded a low matrix strain gradient, and proved for a second time that the interface shear stress was very low if not zero (Fig. 10-a). This observation was valid for the six TRCMC configurations.

To compare the experimental results with the values obtained by applying the law of mixtures, the authors considered the Young's modulus E_1 of the pre-cracking zone. The E_1 modulus was calculated taking into account the uncertainties of the reinforcement ratio V_f, the

Young's moduli E_m of the two matrices characterised in pure tension (same as E_t in Table 3), and that of the reinforcement textile E_f. The uncertainty computation is done as follows:

$$\Delta f = \left|\frac{\partial f}{\partial x_1}\right| \Delta x_1 + \ldots + \left|\frac{\partial f}{\partial x_n}\right| \Delta x_n \quad \textbf{Eq. 3}$$

With "Δf" is the uncertainty of a parameter "f" and "Δx_n" is the uncertainty of a parameter "x_n".

E_1 is calculated by application of the law of mixtures as follows:

$$E_1 = E_f \times V_f + (1 - V_f) \times E_m \quad \textbf{Eq. 4}$$

The uncertainty of E_1 is calculated by applying equation Eq.3 as follows:

$$\Delta E_1 = \left|\frac{\partial E_1}{\partial V_f}\right| \Delta V_f + \left|\frac{\partial E_1}{\partial E_m}\right| \Delta E_m + \left|\frac{\partial E_1}{\partial E_f}\right| \Delta E_f \quad \textbf{Eq. 5}$$

The uncertainty of E_1:

$$\Delta E_1 = (E_f - E_m) \times \Delta V_f + (1 - V_f) \times \Delta E_m + V_f \times \Delta E_f \quad \textbf{Eq. 6}$$

With "ΔE_1" is the uncertainty of "E_1", and "ΔV_f", "ΔE_m" and "ΔE_f" are the standard deviations of "V_f, "E_m" and "E_f", respectively.

The results are summarised in Table 6 and show that for both matrices and the law of mixtures, the higher the reinforcement ratio, the higher the stiffness E_1. A minimal difference is calculated, which corresponds to the difference between the closest limits of the intervals of the experimental values and the law of mixtures in the case where they do not overlap (Fig. 15). Otherwise, there is no difference and therefore the minimum difference is nil. We observed a minimal difference that varied from 0% to 3.35% between the experimental results and the law of mixtures. This difference can be explained by the geometric imperfections of the specimens that influenced the value of the cross-section and therefore the calculated physical quantities.

In conclusion, according to the experimental results, the law of mixtures can be applied to the first zone of the behaviour of the TRCMC on the condition that the geometrical characteristics of the specimen are controlled in a suitable way and that the mechanical properties of the matrix and the textile were established as precisely as possible.

Table 6 : Comparison of stiffness of pre-cracking zone E_1 between experimental results and the law of mixtures

Matrix	M1			M2		
Reinforcement	1 Layer	2 Layers	3 Layers	1 Layer	2 Layers	3 Layers
Reinforcement ratio V_f (%)	2.4 ± 0.18	4.8 ± 0.36	7.2 ± 0.53	2.4 ± 0.18	4.8 ± 0.36	7.2 ± 0.53
E_m matrix (MPa)	10,700 ± 316			14,000 ± 492		
E_f textile (MPa)	35,000 ± 3,180					
Experimental value of E_1 (MPa)	12,300 ± 300	13,200 ± 350	13,800 ± 410	13,200 ± 320	13,500 ± 430	14,800 ± 520
Law of mixtures (MPa) $E_1 = V_f \times E_f + (1-V_f) \times E_m$	11,289 ± 427	11,879 ± 541	12,468 ± 652	14,509 ± 593	15,019 ± 696	15,529 ± 798
Minimal difference (%)	2.37	3.35	2.02	2.93	2.82	0.00

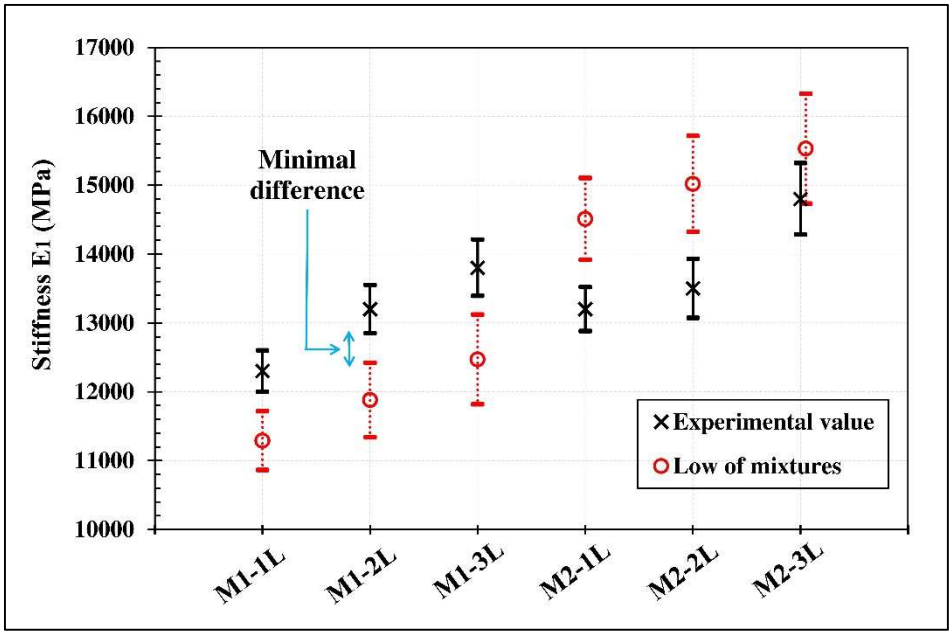

Fig. 15: Evolution of the stiffness E_1 with the standard deviations of the six configurations tested: experimental and law of mixtures values

5.2.Second zone: crack propagation zone

Once the ultimate stress in the matrix is reached, the first crack appears that defines the beginning of the second zone of the tensile behaviour. After that, with an increase in the load, transversal cracks successively occur (Fig. 8-b, c, and d). An instantaneous drop in the stress at

the time of each crack occurrence was noted, followed by an increase in stress, then the occurrence of another crack, and so on (Fig. 11).

The optical fibre segment placed in the matrix measured its normal strain along the specimen including the strain of the optical fibre at the crack location. At these points, the strain peaked and corresponded to the elongation of the optical fibre caused by the opening of the crack and not the strain in the matrix. Referring to the bases of the mechanics at the crack location, the strain in the matrix must be zero. Therefore, an extension of the strain curve obtained by the optical fibre has to be made as shown by the dotted lines in Fig. 16 to obtain the complete curve of the matrix strain. This extension is obtained by extrapolating the points of the experimental curve obtained over the length of the load transfer zone, considering that at the crack location the strain in the matrix is zero. This extension of the matrix strain curves at the crack location is presented on the experimental results shown in Fig. 8-b, c and d.

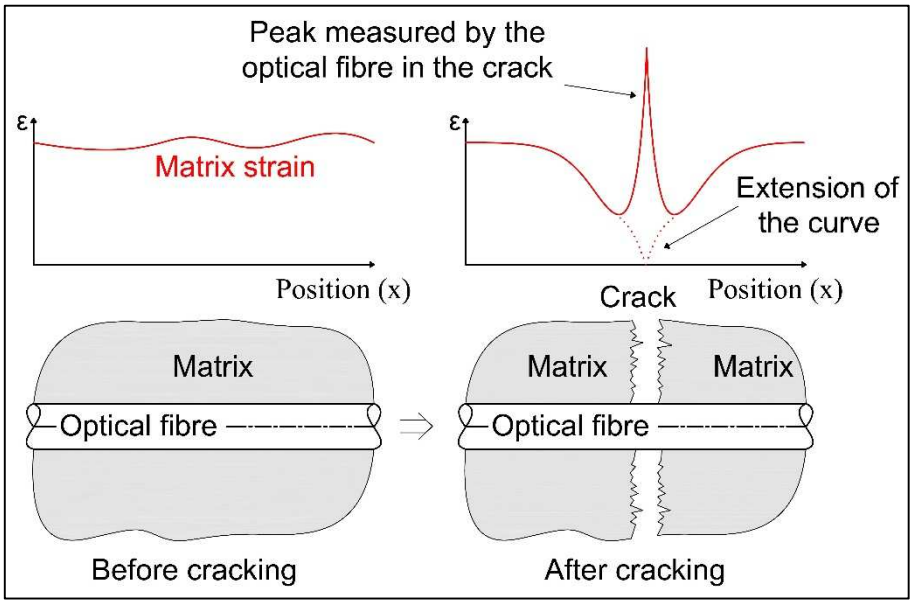

Fig. 16: Adaptation of matrix strain profile at crack position.

Analysing the mechanical behaviour of the matrix and the textile after the appearance of the first crack (Fig. 8-b), and based on the analysis of the previous paragraph, note that the matrix strain gradually recovered from zero at the crack location with a decreasing gradient to the nominal strain value calculated by the law of mixtures corresponding to the stress state generated by the applied load. This incrementation of the strain in the matrix occurred over a distance called the 'load transfer length' denoted as δ_o. On this length, we can consider that the textile/matrix interface was damaged, and therefore the connection was no longer perfect in this

region. However, by considering the mechanical equilibrium of the composite over this distance, the textile supported the force F_f resulting from the total force F_t minus the force supported by the matrix F_m ($F_t = F_m + F_f$). Therefore, at the crack location where the matrix was not loaded, the textile supported all the internal force, which explains the peak of the textile strain curve at the crack location (Fig. 8-b, c, and d). Therefore, at a distance δ_o from the crack, the strain in the matrix increased and the force supported by the matrix increased, by making the mechanical equilibrium, the force supported by the textile along the distance δ_o decreases. This explains the decreasing trend in the strain of the textile from the peak recorded at the crack to δ_o.

Cracks in the composite occurred where the ultimate matrix strain was reached, and therefore, over the length δ_o, the strain was lower compared to the rest of the matrix. This implies that, with an increase in the stress, the ultimate matrix strain will be reached in the region outside the δ_o area induced by previous cracks. From this analysis, it can be concluded that the crack spacing cannot be less than δ_o. Thus, as long as the spacing between two adjacent cracks is greater than 2 δ_o, another crack will occur between them. Once the crack spacing has fallen below 2 δ_o, the two load transfer lengths of the two cracks overlap, and the matrix strain cannot reach its ultimate value to crack again in this area. Once all spacing between two adjacent cracks in the matrix become shorter than 2 δ_o, no further cracks can appear, declaring the end of the crack propagation zone and the beginning of the third zone, the post-cracking zone.

In conclusion, as shown in Fig. 8, the final cracking pattern depends on the value of δ_o with a final crack spacing (X) between δ_o and 2 δ_o as

$$\delta_o < X \leq 2\,\delta_o. \qquad \textbf{Eq. 7}$$

This final cracking scheme allows the estimation of δ_o based on the smallest spacing between two adjacent cracks X_{min} and the largest spacing X_{max}. Eq.7 implies that:

$$\delta_o < X_{min} \text{ and } X_{max} \leq 2\,\delta_o. \qquad \textbf{Eq. 8}$$

Therefore, the load transfer length is within the range of

$$X_{max}/2 \leq \delta_o < X_{min}. \qquad \textbf{Eq. 9}$$

According to the cracking pattern observed in Fig. 14, the crack spacing decreased with an increase in the number of reinforcement layers. From this observation and based on Eq. 9, we can conclude that δ_o decreases with an increase in the reinforcement ratio without being able to quantify it precisely.

The values of δ_o at the cracking time were precisely measurable for the six tested configurations owing to the optical fibre measurements. The results are summarised in Table 7. The average and standard deviations were obtained by comparing the value of δ_o of each of the

six segments of optical fibre located inside the specimens. The evolution of δ_o according to the type of matrix and the reinforcement ratio is presented in Fig. 17. These results lead to the conclusion that the load transfer length depends on the type of matrix and gradually decreases with an increase in the reinforcement ratio. The effect of the type of matrix can be seen by considering a given stress, and calculating the load transfer length for the six configurations for the same stress referring to Fig. 17-b. For example, for a stress of 4 MPa, we will find 35 mm for M1-1L and 25 mm for M2-1L (difference of 28%); 25 mm for M1-2L and 20 for M2-2L (difference of 20%); 10 mm for M1-3L and 5 for M2-3L (difference of 50%).

Table 7: Load transfer length and maximum interface stress at time of cracking and maximum–minimum crack spacing of specimen after the test.

	Matrix M1			Matrix M2		
	1 Layer	2 Layers	3 Layers	1 Layer	2 Layers	3 Layers
δo (mm)	31.2	22.1	5.7	27	23.7	8.05
Standard deviation	2.2	0	0.5	0.5	0.14	0.9
Variation coefficient (%)	7.05	0.00	8.77	1.85	0.59	11.18
τ_{max} (MPa)	2.37	1.8	2	4.73	2.57	3.5
X_{min} (mm)	34	24	7	35	24	10
X_{max} (mm)	48	40	10	55	45	16

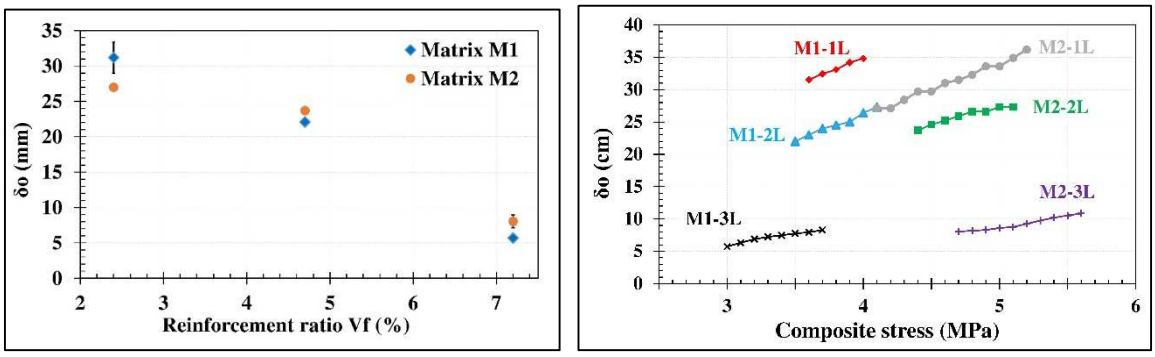

a b

Fig. 17: Evolution of load transfer length: (a) at the time of cracking according to type of matrix and reinforcement ratio; (b) between the time of appearance of the first and second crack, as a function of the stress applied to the composite.

In terms of the shear stress at the textile/matrix interface over the distance δ_o, on the left side of the crack the matrix strain decreased gradually to zero (Fig. 8-b). Therefore, the strain gradient on this area was negative, which explains the negative value of the stress at the interface (Fig. 10-b). In addition, over the distance δ_o on the right side of the crack, the strain in the matrix gradually increased to a fixed nominal value. Therefore, the strain gradient on this

zone was positive, thus explaining the positive value of the interface stress in this region. In the zones where the strain in the matrix was constant, the gradient was zero, implying a null interface shear stress. The non-linear shape of the interface stress shown in Fig. 10-b, c, and d owing to the decrease in the absolute value of the matrix strain gradient when moving away from the crack is shown in Fig. 9.

As previously mentioned, the crack propagation zone is characterised by a force drop when a crack occurs. Similarly, in the experimental results shown in Fig. 8, 8, and 9, the local strain in the matrix decreased during cracking, while the textile strain increased over a distance of $\pm\delta_o$ and decreased over the rest of the specimen. However, in this study and in literature, the global behaviour of a TRCMC is characterised by a total force (or stress) drop during cracking, but the strain is considered constant at this point [1]. This difference between the global and local behaviour of a TRCMC can be explained as follows: the tensile test is generally displacement controlled, and therefore, at the cracking time, the global elongation ΔL remains the same before and after cracking leading to a global strain value corresponding to the crack appearance (Fig. 18). However, the occurrence of a crack (and therefore a load transfer length δ_o) changed the geometric characteristics of the specimen and constituted a 'δ_o - crack - δ_o' zone less rigid than the rest of the uncracked specimen. This change produced a new TRCMC material with serial regions that can be of two types: the 'δo - crack - δo' regions with a stiffness E lower than E_1, and the areas not covered by the load transfer lengths of the cracks that appeared, with a stiffness E_1. This results in an equivalent global Young's modulus E_{equ} less than E_1 ($E_{equ} < E_1$), and therefore, by applying Hooke's law ($\sigma = E \times \varepsilon$),

$$\varepsilon_{total} = \frac{\Delta L}{L} = \frac{\sigma}{E} = \frac{\sigma_{Before\ cracking}}{E_1} = \frac{\sigma_{After\ cracking}}{E_{equ}} \quad \textbf{Eq. 10}$$

Since $E_{equ} < E_1$, we deduce that

$$\frac{\sigma_{After\ cracking}}{\sigma_{Before\ cracking}} = \frac{E_{equ}}{E_1} < 1. \quad \textbf{Eq. 11}$$

This implies that

$$F_{After\ cracking} < F_{Before\ cracking}, \quad \textbf{Eq. 12}$$

and hence the drop-in stress when cracks appear. This drop subsequently induces a smaller composite stress in all cross-sections of the TRCMC and a lower local strain than that before cracking, which leads to a drop in local strain of the matrix and textile in the uncracked regions. However, in the 'δ_o - crack - δ_o' zone, the textile supports a greater internal force than that before cracking, and therefore its strain increases in this zone expressed by the peaks in Fig. 8-b, c, and d and by an instantaneous increase in the textile strain at the crack location as shown in Fig. 11.

From a mechanical point of view, the global behaviour of a TRCMC results from the combination of the local behaviour of the matrix and the textile on the entire specimen. In Fig. 11, the second zone of the local behaviour of the textile and matrix overlaps with the first zone on one side and with the third zone on the other side and cannot be approached by an E_2 module equivalent to that of global behaviour. In addition, if we consider only the behaviour of a part of the TRCMC, we find that its second zone is different from that of the global behaviour of the entire specimen and actually depends on the measurement technique, the measurement area, and the number of considered cracks. From this study we can deduce that the different values of E_2 obtained in literature [7,12] were the result of a change in either the measurement region or the extensometry technique. To estimate an equivalent rigidity E_{eq} of the crack propagation zone of a specimen, E_{eq} must be associated with the global and not the local behaviour. To do this, it is necessary to use measurement devices that allow to have the global behaviour, such as LVDTs, over the entire length of the specimen. In addition, it is necessary to indicate the length of the specimen and the number of cracks occurred during the test.

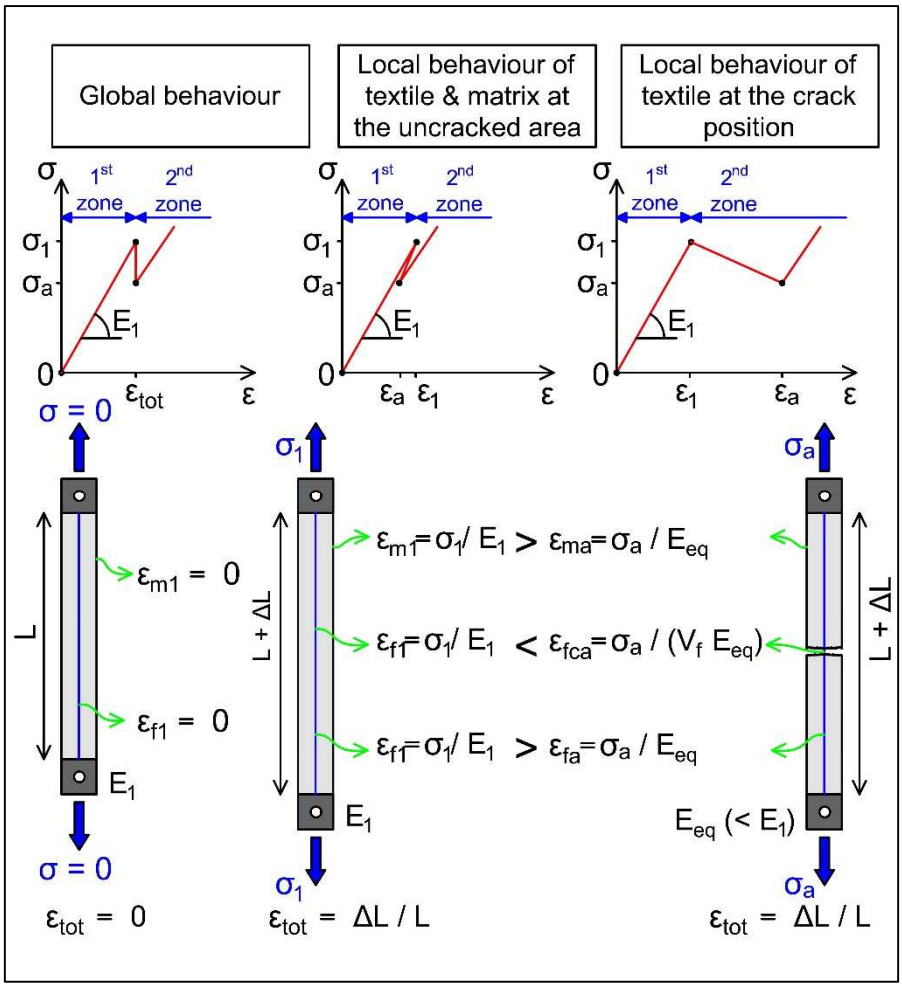

Fig. 18: Diagram of difference between local and global behaviour of the TRCMC in the crack propagation zone.

5.3.Third zone: post-cracking zone

At this phase of mechanical behaviour of a TRCMC in tension, the textile supports the applied load. As the matrix/textile interface is damaged, the load transfer between these two components in this zone is performed by friction. The matrix remains tensioned but its strain no longer increases or decreases even slightly, and therefore no further cracks are formed. However, it can be considered that the textile strain increases linearly with an increase in the load.

To compare the tensile behaviour of the textile at the core of the TRCMC in the post-cracking zone with that of the textile alone, the comparison of the Young's modulus values is summarised in Table 8. The stiffness E_3 values are computed as the slope of the third branch of the textile stress-strain curves depicted in Fig. 9. To obtain the Young's modulus of reinforcement at the core of the TRCMC (E_{3f}), the composite modulus E_3 is divided by the reinforcement ratios V_f.

Table 8: Comparison of textile stiffness at core of TRCMC and stiffness of textile alone

Matrix	M1			M2		
Number of layers	1 Layer	2 Layers	3 Layers	1 Layer	2 Layers	3 Layers
E_3 (MPa)	760	1,600	2,700	800	1,700	2,600
V_f (%)	2.4	4.8	7.2	2.4	4.8	7.2
Experimental value $E_{f\,exp} = E_3 / V_f$ (MPa)	31,667	33,333	37,500	33,333	35,417	36,111
$E_{f\,fibre}$ alone (MPa)	35,000 ± 3,180					
$E_{f\,exp}$ included in uncertainty interval of $E_{f\,fibre}$?	✓	✓	✓	✓	✓	✓

Based on these results, it can be concluded that in the third zone, the textile supports the entire load applied to the composite. The equivalent internal force is the sum of that applied during the first and second zones to constitute the total force supported by the textile. However, the matrix generally held the strain value after the occurrence of the last crack. This behaviour explains the increase in crack openings observed during this phase. It should be noted that the research was only of a short-term nature, so it is advisable to assess in the long term if the matrix strain will not decrease.

5.4.Summary of observed behaviours

To outline and summarise the mechanical behaviour of a TRCMC in tension, a simplified overview of the evolution of the strain and stress in the textile and matrix and the shear stress

at the textile/matrix interface is shown in Fig. 19. σ_a, σ_b, σ_c, σ_d in Fig. 19 correspond to the stress in the composite at the time of the appearance of the 1st, 2nd, 3rd, 4th crack, respectively. This figure shows that in terms of strain, when in a zone of the TRCMC the strain in the textile is close to that in the matrix, the probability that a crack will appear in this zone is very high. This means that the transition to the post-cracking zone will only be achieved if at any point in the TRCMC, the textile strain becomes greater than that of the matrix. In terms of shear stress at the interface, the same analysis can be done. The more the shear stress is nil in a zone, the more the probability of a new crack to appear in this zone is higher. The transition to the post-cracking zone is made once the shear stress becomes different from zero in each point of the textile/matrix interface of the TRCMC.

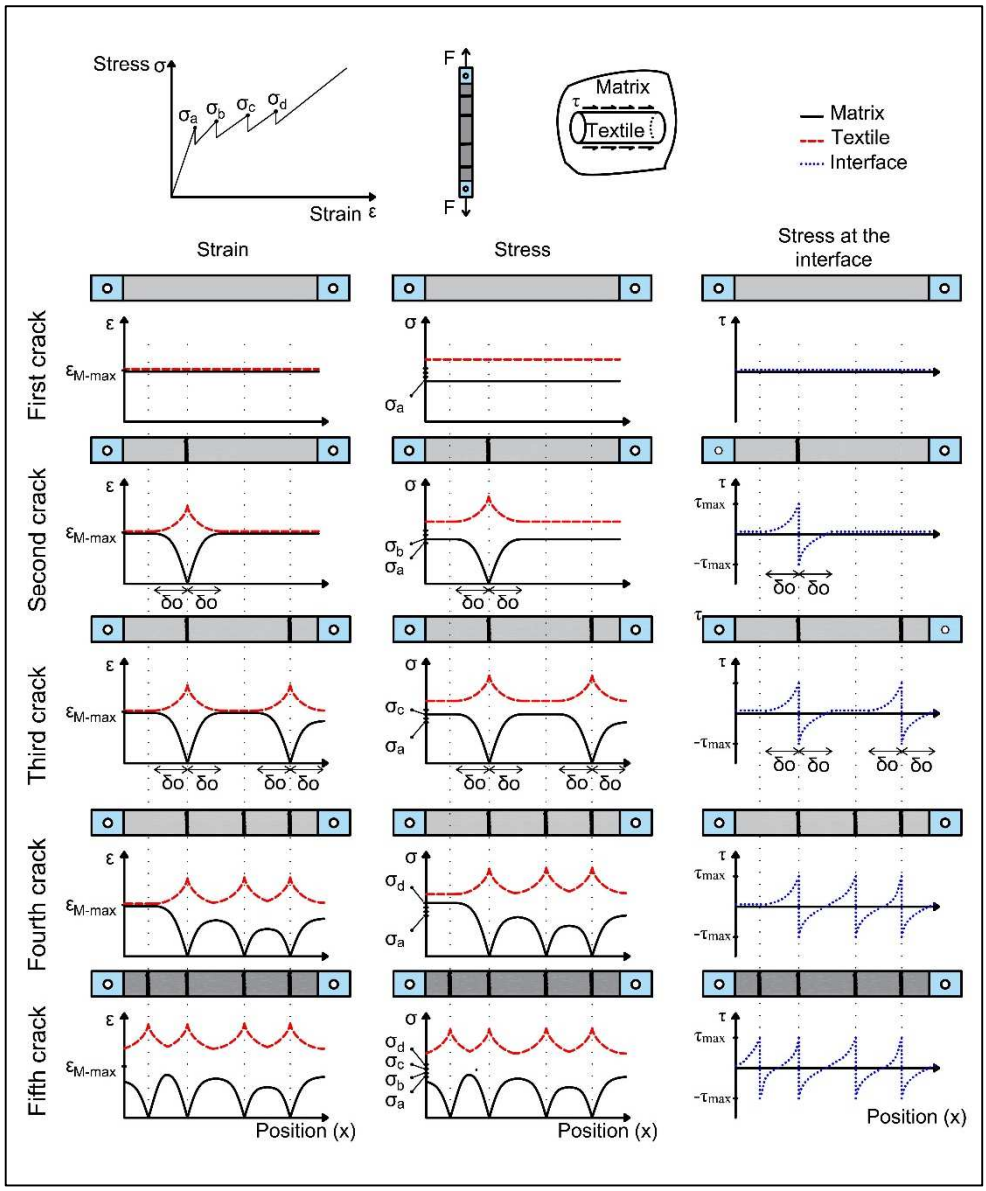

Fig. 19: Diagram of longitudinal strain and stress distribution of textile and matrix and stress at the interface between the two components.

6. Conclusions and outlook

Experimentally, the local and global tensile behaviours of TRCMC were investigated using distributed optical fibres as strain sensors embedded in the core of the composites. Six configurations were tested and analysed with two different matrices and three reinforcement ratios.

Utilising optical fibre measurements, the behaviour of the matrix, textile, and textile/matrix interface during the three zones of mechanical behaviour of typical TRCMCs in tension were measured, identified, and analysed. The main results are:

- In the pre-cracking zone of the TRCMC, the mechanical behaviour of the matrix and the textile reinforcement are approximately identical and characterised by a quasi-linear stiffness and no stress at the textile/matrix interface. The validity of the law of mixtures in this zone was demonstrated, and the hypothesis of a perfect bond between the matrix and textile was validated.
- In the crack propagation zone, the parameter 'load transfer length' δ_o controls the number and appearance of cracks and the end of this zone. Thus, over a length δ_o in the vicinity of a crack, the matrix strain decreases until it becomes nil at the crack location, and the textile supports the entire stress at this location.
- The parameter 'load transfer length' δ_o depends on the characteristics of the matrix and decreases with an increase in the reinforcement ratio.
- The shear stress distribution at the textile/matrix interface has a non-linear shape over the load transfer length. It decreases from a crack at a distance equal to δ_o, after which it is equal to zero.
- The force drop at the cracking time of a TRCMC and the difference in local and global behaviours are a result of changes in the local and global equivalent stiffness of a TRCMC.
- In the post-cracking zone, the textile supports almost all the load applied during this stage, but the matrix remains stretched while keeping the strain cumulated during the two previous zones. The textile/matrix interface is supposed to be damaged, and the force transmission between these two components is caused by friction.
- From an experimental point of view, the tensile test took approximately an hour and generated a post-processing data file of approximately 100 GB because the loading velocity was quite low (100 µm/min) and the optical acquisition system recorded at a default frequency of 100 Hz. In addition, there were a large number of measurement

points on the optical fibre. As a consequence, the required time for the analysis of results was onerous.

- Looking at the textile strain distribution along the specimens, especially before cracking, no information could be linked to the transverse fibres of the textile. In future studies, it would be interesting to investigate the transverse fibres by optical fibres to identify the complete behaviour of the reinforcement grid.
- The textile reinforcement used in this study was pre-impregnated and had a monolithic behaviour, i.e. all its filaments behaved in the same way. As an outlook, we propose to use optical fibre to study the mechanical behaviour of a TRCMC reinforced with multifilament yarn textile to present telescopic behaviour, and thus more complex phenomena at the interface can be considered.
- This work is based on gluing a segment of the optical fibre to one of the longitudinal fibres of the textile reinforcement. It would be interesting to glue an optical fibre to all these longitudinal fibres to study the working ratio of each fibre before, during and after crack propagation.
- A part of the post-cracking zone, the ultimate stress and ultimate strain of the composite were not investigated due to the sliding of the textile reinforcement in the matrix at the positions of the aluminium plates. In future work, it would be wise to carry out a series of tests to determine the proper anchor length of the aluminium plates to ensure textile failure and study the entire post-cracking zone including the ultimate stress and ultimate strain of the composite using optical fibres.
- As an outlook, we propose to investigate the behaviour of TRCMCs with force-controlled tensile behaviour. Also, it would be interesting to study in details the load transfer length as a function of the mechanical and geometrical parameters of the TRCMC components, as well as the cracks' opening along the test and the influence of the number of textiles on matrix strains along the thickness of the specimens.
- This work demonstrates the possibility of extending a load transfer study by setting up measurements with no-contact zones between the matrix, textile, and optical fibre to accurately characterise the distribution of the load transfer length during tensile tests.

References

[1] V. Mechtcherine, Novel cement-based composites for the strengthening and repair of

concrete structures, Constr. Build. Mater. 41 (2013) 365–373. doi:10.1016/J.CONBUILDMAT.2012.11.117.

[2] G. Promis, T.Q. Bach, A. Gabor, P. Hamelin, Failure behavior of E-glass fiber- and fabric-reinforced IPC composites under tension and compression loading, Mater. Struct. 47 (2014) 631–645. doi:10.1617/s11527-013-0085-6.

[3] R. Ortlepp, S. Ortlepp, Textile reinforced concrete for strengthening of RC columns: A contribution to resource conservation through the preservation of structures, Constr. Build. Mater. 132 (2017) 150–160. doi:10.1016/J.CONBUILDMAT.2016.11.133.

[4] L.A.S. Kouris, T.C. Triantafillou, State-of-the-art on strengthening of masonry structures with textile reinforced mortar (TRM), Constr. Build. Mater. 188 (2018) 1221–1233. doi:10.1016/J.CONBUILDMAT.2018.08.039.

[5] M. Sánchez, P. Faria, L. Ferrara, E. Horszczaruk, H.M. Jonkers, A. Kwiecień, J. Mosa, A. Peled, A.S. Pereira, D. Snoeck, M. Stefanidou, T. Stryszewska, B. Zając, External treatments for the preventive repair of existing constructions: A review, Constr. Build. Mater. 193 (2018) 435–452. doi:10.1016/J.CONBUILDMAT.2018.10.173.

[6] P.D. Askouni, C. (Corina) G. Papanicolaou, Textile Reinforced Mortar-to-masonry bond: Experimental investigation of bond-critical parameters, Constr. Build. Mater. 207 (2019) 535–547. doi:10.1016/J.CONBUILDMAT.2019.02.102.

[7] R. Contamine, A. Si Larbi, P. Hamelin, Contribution to direct tensile testing of textile reinforced concrete (TRC) composites, Mater. Sci. Eng. A. 528 (2011) 8589–8598. doi:10.1016/J.MSEA.2011.08.009.

[8] B. Mobasher, A. Peled, J. Pahilajani, Distributed cracking and stiffness degradation in fabric-cement composites, Mater. Struct. 39 (2007) 317–331. doi:10.1007/s11527-005-9005-8.

[9] J. Hegger, S. Voss, Investigations on the bearing behaviour and application potential of textile reinforced concrete, Eng. Struct. 30 (2008) 2050–2056. doi:10.1016/J.ENGSTRUCT.2008.01.006.

[10] A. Peled, Z. Cohen, Y. Pasder, A. Roye, T. Gries, Influences of textile characteristics on the tensile properties of warp knitted cement based composites, Cem. Concr. Compos. 30 (2008) 174–183. doi:10.1016/J.CEMCONCOMP.2007.09.001.

[11] G. Promis, A. Gabor, P. Hamelin, Analytical modeling of the bending behavior of textile reinforced mineral matrix composite beams, Compos. Struct. 93 (2011) 792–801. doi:10.1016/J.COMPSTRUCT.2010.08.002.

[12] O. Homoro, X.H. Vu, E. Ferrier, Experimental and analytical study of the thermo-mechanical behaviour of textile-reinforced concrete (TRC) at elevated temperatures: Role of discontinuous short glass fibres, Constr. Build. Mater. 190 (2018) 645–663. doi:10.1016/J.CONBUILDMAT.2018.09.142.

[13] C. Caggegi, E. Lanoye, K. Djama, A. Bassil, A. Gabor, Tensile behaviour of a basalt TRM strengthening system: Influence of mortar and reinforcing textile ratios, Compos. Part B Eng. 130 (2017) 90–102. doi:10.1016/J.COMPOSITESB.2017.07.027.

[14] C. Caggegi, D. Sciuto, M. Cuomo, Experimental study on effective bond length of basalt textile reinforced mortar strengthening system: Contributions of digital image correlation, Measurement. 129 (2018) 119–127. doi:10.1016/J.MEASUREMENT.2018.07.003.

[15] M. Cao, Y. Mao, M. Khan, W. Si, S. Shen, Different testing methods for assessing the synthetic fiber distribution in cement-based composites, Constr. Build. Mater. 184 (2018) 128–142. doi:10.1016/J.CONBUILDMAT.2018.06.207.

[16] J. Gao, A. Sha, Z. Wang, L. Hu, D. Yun, Z. Liu, Y. Huang, Characterization of carbon fiber distribution in cement-based composites by Computed Tomography, Constr. Build. Mater. 177 (2018) 134–147. doi:10.1016/J.CONBUILDMAT.2018.05.114.

[17] B.K. Ahn, W.A. Curtin, Strain and hysteresis by stochastic matrix cracking in ceramic matrix composites, J. Mech. Phys. Solids. 45 (1997) 177–209. doi:10.1016/S0022-5096(96)00081-6.

[18] H. Cuypers, J. Wastiels, Stochastic matrix-cracking model for textile reinforced cementitious composites under tensile loading, Mater. Struct. Constr. 39 (2006) 777–786. doi:10.1617/s11527-005-9053-0.

[19] W. Hawkins, J. Orr, T. Ibell, P. Shepherd, An Analytical Failure Envelope for the Design of Textile Reinforced Concrete Shells, Structures. 15 (2018) 56–65. doi:10.1016/J.ISTRUC.2018.06.001.

[20] R. Contamine, Contribution à l'étude du comportement mécanique de composites

textile-mortier : application à la réparation et/ou renforcement de poutres en béton armé vis-à-vis de l'effort tranchant, (2011).

[21] U. Dilthey, Application of polymers in textile reinforced concrete – From the interface to construction elements, in: ICTRC'2006 - 1st Int. RILEM Conf. Text. Reinf. Concr., RILEM Publications SARL, 2006: pp. 55–64. doi:10.1617/2351580087.006.

[22] O. Homoro, M. Michel, T.N. Baranger, Pull-out response of glass yarn from ettringite matrix: Effect of pre-impregnation and embedded length, Compos. Sci. Technol. 170 (2019) 174–182. doi:10.1016/J.COMPSCITECH.2018.11.045.

[23] J. Dupont, Comportements de Capteurs à Fibres Optiques, noyés ou fixés en surface d'ouvrages en béton, Ecole des Ponts ParisTech, 2002.

[24] A. Tixier, C. Rospars, F. Dufour, A. Khadour, B. Masson, Analyse des déformations par fibres optiques le long de l'interface acier-béton dans un essai push-in, in: 31èmes Rencontres de l'AUGC, ENS Cachan, France, 2013.

[25] F. Ansari, State-of-the-art in the applications of fiber-optic sensors to cementitious composites, Cem. Concr. Compos. 19 (1997) 3–19. doi:10.1016/S0958-9465(96)00038-8.

[26] Y.. Rao, Recent progress in applications of in-fibre Bragg grating sensors, Opt. Lasers Eng. 31 (1999) 297–324. doi:10.1016/S0143-8166(99)00025-1.

[27] J.-M. Henault, Approche méthodologique pour l'évluation des performances et de la durabilité des systèmes de mesure réparties de déformation : application à un câble à fibre optique noyé dans le béton, Université Paris-Est-France, 2013.

[28] Q. Li, G. Li, G. Wang, L. Yuan, CTOD measurement for cracks in concrete by fiber optic sensors, Opt. Lasers Eng. 42 (2004) 377–388. doi:10.1016/J.OPTLASENG.2004.03.002.

[29] D. Li, L. Ren, H. Li, Mechanical Property and Strain Transferring Mechanism in Optical Fiber Sensors, in: Fiber Opt. Sensors, InTech, 2012. doi:10.5772/27731.

[30] W. Du, X.M. Tao, H.Y. Tam, C.L. Choy, Fundamentals and applications of optical fiber Bragg grating sensors to textile structural composites, Compos. Struct. 42 (1998) 217–229. doi:10.1016/S0263-8223(98)00045-2.

[31] L. Bruno, Mechanical characterization of composite materials by optical techniques: A review, Opt. Lasers Eng. 104 (2018) 192–203. doi:10.1016/J.OPTLASENG.2017.06.016.

[32] M. Saidi, A. Gabor, Use of distributed optical fibre as a strain sensor in textile reinforced cementitious matrix composites, Measurement. 140 (2019) 323–333. doi:10.1016/j.measurement.2019.03.047.

[33] I. De Baere, G. Luyckx, E. Voet, W. Van Paepegem, J. Degrieck, On the feasibility of optical fibre sensors for strain monitoring in thermoplastic composites under fatigue loading conditions, Opt. Lasers Eng. 47 (2009) 403–411. doi:10.1016/J.OPTLASENG.2008.01.001.

[34] X. Li, C. Zhao, J. Lin, S. Yuan, The internal strain of three-dimensional braided composites with co-braided FBG sensors, Opt. Lasers Eng. 45 (2007) 819–826. doi:10.1016/J.OPTLASENG.2006.12.003.

[35] J.H.L. Grave, M.L. Håheim, A.T. Echtermeyer, Measuring changing strain fields in composites with Distributed Fiber-Optic Sensing using the optical backscatter reflectometer, Compos. Part B Eng. 74 (2015) 138–146. doi:10.1016/J.COMPOSITESB.2015.01.003.

[36] J.E. Woods, D.T. Lau, X. Bao, W. Li, Measuring strain fields in FRP strengthened RC shear walls using a distributed fiber optic sensor, Eng. Struct. 152 (2017) 359–369. doi:10.1016/J.ENGSTRUCT.2017.09.034.

[37] A. Skontorp, Effect of embedded optical fibers on the structural integrity of composites, (2000).

[38] A. Barrias, J.R. Casas, S. Villalba, Distributed optical fibre sensors in concrete structures: Performance of bonding adhesives and influence of spatial resolution, Struct. Control Heal. Monit. 26 (2019) e2310. doi:10.1002/stc.2310.

[39] B.J. Soller, D.K. Gifford, M.S. Wolfe, M.E. Froggatt, High resolution optical frequency domain reflectometry for characterization of components and assemblies, Opt. Express. 13 (2005) 666. doi:10.1364/OPEX.13.000666.

[40] BS EN 196-1, Methods of testing cement–Part 1: Determination of strength, European Committee for standardization, 2005.

[41] R. Contamine, A. Si Larbi, P. Hamelin, Identifying the contributing mechanisms of textile reinforced concrete (TRC) in the case of shear repairing damaged and reinforced concrete beams, Eng. Struct. 46 (2013) 447–458. doi:10.1016/J.ENGSTRUCT.2012.07.024.